Saudi Pharmaceutical Journal 32 (2024) 102062

HOSTED BY

Contents lists available at ScienceDirect

Saudi Pharmaceutical Journal

journal homepage: www.sciencedirect.com

Unveiling potent Schiff base derivatives with selective xanthine oxidase inhibition: *In silico* and *in vitro* approach

Fatna Bellahcene [a], Khedidja Benarous [a,*], Arif Mermer [b,c,d], Houssem Boulebd [e], Talia Serseg [a,f], Abderahmane Linani [a], Alaeddine Kaouka [f], Mohamed Yousfi [a], Asad Syed [g], Abdallah M. Elgorban [g], Yasuhiro Ozeki [h], Sarkar M.A. Kawsar [i]

[a] *Laboratory of Fundamental Sciences, Faculty of Sciences, University of Amar Telidji, Laghouat, Algeria*
[b] *Department of Biotechnology, University of Health Sciences, İstanbul, Turkey*
[c] *Experimental Medicine Application and Research Center, Validebag Research Park, University of Health Sciences, İstanbul, Turkey*
[d] *Department of Pharmacy, University of Health Sciences, İstanbul, Turkey*
[e] *Department of Chemistry, Faculty of Exact Sciences, University of Constantine 1, Constantine, Algeria*
[f] *Laboratoire des Sciences Appliquées et Didactiques, Ecole Normale Supérieure de Laghouat, Algeria*
[g] *Department of Botany and Microbiology, College of Science, King Saud University, P.O. 2455, Riyadh 11451, Saudi Arabia*
[h] *Graduate School of NanoBio Sciences, Yokohama City University, 22-2 Seto, Kanazawa-ku, Yokohama 236-0027, Japan*
[i] *Laboratory of Carbohydrate and Nucleoside Chemistry, Department of Chemistry, Faculty of Science, University of Chittagong, Chittagong 4331, Bangladesh*

ARTICLE INFO

Keywords:
Schiff base
Triazole
Gout
Xanthine oxidase inhibition
In silico approach

ABSTRACT

This research describes the synthesis by an environmentally-friendly method, microwave irradiation, development and analysis of three novel and one previously identified Schiff base derivative as a potential inhibitor of bovine xanthine oxidase (BXO), a key enzyme implicated in the progression of gout. Meticulous experimentation revealed that these compounds (**10**, **9**, **4**, and **7**) have noteworthy inhibitory effects on BXO, with IC50 values ranging from 149.56 μM to 263.60 μM, indicating their good efficacy compared to that of the standard control. The validation of these results was further enhanced through comprehensive in silico studies, which revealed the pivotal interactions between the inhibitors and the catalytic sites of BXO, with a particular emphasis on the imine group (-C = N-) functionalities. Intriguingly, the compounds exhibiting the highest inhibition rates also showcase advantageous ADMET profiles, alongside encouraging initial assessments via PASS, hinting at their broad-spectrum potential. The implications of these findings are profound, suggesting that these Schiff base derivatives not only offer a new vantage point for the inhibition of BXO but also hold considerable promise as innovative therapeutic agents in the management and treatment of gout, marking a significant leap forward in the quest for more effective gout interventions.

1. Introduction

The term “Schiff base” originates from the name of the German chemist Hugo Schiff, who first described the compounds produced by the reaction between primary amines and carbonyl compounds (Raczuk et al., 2022). Schiff bases play a crucial role as ligands and are among the most widely used organic substances (Boulechfar et al., 2023, Khan et al., 2023, Luo et al., 2023). They can be considered a subclass of imines (Ahmad et al., 2022, Shilpa Laxman, 2022), which contain the imine (-C = N-) group in their structure that occurs through the reaction of an aldehyde or ketone with a primary amine under suitable conditions (Ahmad et al., 2022, Nuriye Tuna, 2022). The imine group can be part of the 1,2,4-triazole ring (Jumaa et al., 2017). In this instance, the compounds demonstrated an enhanced ability to donate a pair of electrons through their azomethine group (Nuriye Tuna, 2022, Zhou et al., 2022). Schiff bases exhibit a range of biological activities. In particular, they exhibit antifungal (Dong et al., 2023), anticancer (Matela, 2020), anti-tumor (Li et al., 2012), anti-inflammatory (Azim et al., 2021), and antioxidant (Saadaoui et al., 2019) activities. In addition, it has been suggested that the azomethine linkage might be responsible for their

Peer review under responsibility of King Saud University.
* Corresponding author.
E-mail address: k.benarous@lagh-univ.dz (K. Benarous).

https://doi.org/10.1016/j.jsps.2024.102062
Received 24 February 2024; Accepted 2 April 2024
Available online 4 April 2024

biological activities (Saadaoui et al., 2019).

Gout is the most common form of inflammatory arthritis (Newberry et al., 2017, Kim et al., 2023). It is caused by the deposition of monosodium urate (MSU) crystals in articular and nonarticular structures. The major cause of gout is a high serum urate concentration (Dalbeth et al., 2021). In recent years, the prevalence of hyperuricemia has increased due to the increase in the intake of high-purine foods, leading to the overactivity of xanthine oxidase (XO) (Zhao et al., 2019, Yu et al., 2022). Xanthine oxidase is a pivotal enzyme in purine metabolism that catalyzes the conversion of hypoxanthine to xanthine and subsequently to uric acid, thereby increasing the risk of gout. The increase in diseases associated with its overactivity is expected to significantly impact human health and exert substantial pressure on the medical system. Allopurinol and febuxostat are two inhibitors of xanthine oxidase; however, their use is associated with adverse side effects. Nevertheless, they are associated with negative side effects (Zhao et al., 2022). Therefore, the discovery of both natural and synthetic compounds as XO inhibitors is critical.

This study aimed to evaluate, for the first time, the anti-gout activity of twelve Schiff base derivatives (Fig. 1) utilizing the double enzyme detection (DED) method. This was followed by in silico prediction using molecular docking with AutoDock Vina software, assessment of ADMET pharmacokinetic (PK) properties using the preADMET server, and a PASS study.

2. Experimental

2.1. Chemicals and equipment

The bovine milk for the study was sourced from a reputable dairy farm located in Laghouat, Algeria. Uricase and peroxidase enzymes were purchased from BioLab. The substrate (xanthine), K_2HPO_4, KH_2PO_4, HCl, DMSO (dimethyl sulfoxide), EDTA (ethylene diamine tetraacetic acid), trisaminomethane ($C_4H_{11}NO_3$), and all other reagents were purchased from Sigma–Aldrich. Allopurinol (control) was purchased from a local pharmacy. All reagents utilized in the experiment were of analytical grade. Fourier transform infrared (FTIR) spectra were recorded using a Thermo Fisher Scientific Nicolet IS50 FTIR spectrometer. ^{1}H NMR and ^{13}C NMR (APT) spectra were recorded on a Bruker Avance II 400 MHz NMR spectrometer (chemical shift in ppm downfield from TMS (tetramethylsilane) as an internal reference). The mass spectra were obtained by MALDI-TOF/MS (Bruker UltraFleXtreme). A Thermo Fisher Scientific microplate reader was used. A refrigerated centrifuge from HETTICH ROTANTA 460R was used.

2.2. Chemistry

2.2.1. General method for the synthesis of compounds 6–8

A mixture of 1-(4-amino-4H-1,2,4-triazole-3-thion-5-yl)methyl-1H-benzotriazole (10 mmol) and the corresponding aldehyde (10 mmol) in AcOH:H_2O was irradiated in a Monomode MW reactor at 200 °C for 25 min. After completion of the reaction (the progress of the reaction was followed by TLC), the mixture was left cold for 24 h, and the solid formed was filtered by washing with cold water. The crude compounds were purified by recrystallization using an appropriate solvent.

3-[(1H-1,2,3-Benzotriazol-1-yl)methyl]-4-[(furan-2-yl)methylidene] amino]-4,5-dihydro-1H-1,2,4-triazole-5-thione ***(6)***.

FT-IR (υ_{max}, cm^{-1}): 3045 (*ar*-CH), 1568, 1595 and 1633 (C = N). ^{1}H NMR (DMSO-d_6, δppm): 6.14 (s, 2H, CH_2), 6.74 (d, 1H, J = 3.2 Hz, CH), 7.24 (d, 1H, J = 4.0 Hz, CH), 7.39 (t, 1H, J = 8.0 Hz, arH), 7.53 (t, 1H, J = 8.0 Hz, arH), 7.91 (d, 1H, J = 8.0 Hz, arH), 8.01 (s, 1H, CH), 8.03 (d, 1H, J = 3.6 Hz, arH), 9.83 (s, 1H, CH), 14.06 (s, 1H, SH). ^{13}C NMR (DMSO-d_6, δppm): 42.48, 111.49, 113.48, 119.53, 120.80, 124.58, 127.97, 133.63, 145.43, 146.66, 147.46, 148.65, 151.72, 162.41. MALDI-TOF-MS: 326.10458 ($[M + 1]^+$). MALDI-TOF-MS: 325.29327 ([M] +).

3-[(1H-1,2,3-Benzotriazol-1-yl)methyl]-4-[(thiophene-2-yl)methyl-idene]amino]-4,5-dihydro-1H-1,2,4-triazole-5-thione ***(7)***.

FT-IR (υ_{max}, cm^{-1}): 3037 (*ar*-CH), 1571, 1598 and 1648 (C = N). ^{1}H NMR (DMSO-d_6, δppm): 6.14 (s, 2H, CH_2), 7.20 (t, 1H, J = 4.4 Hz, CH),

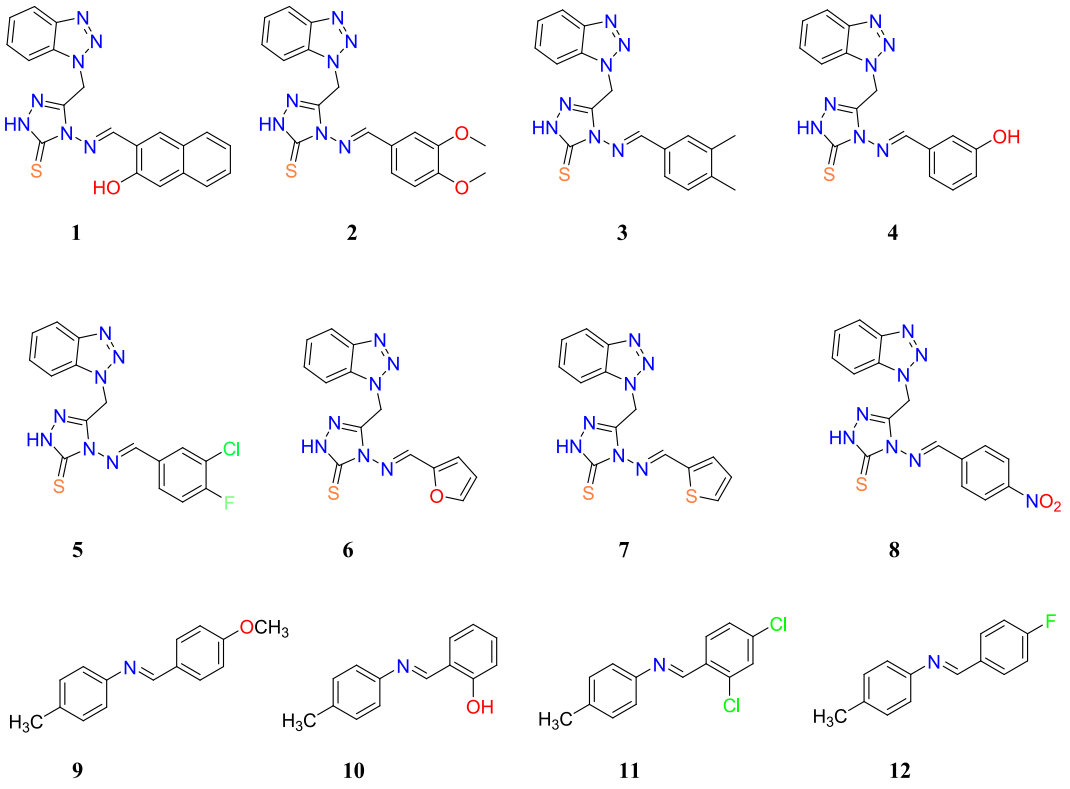

Fig. 1. The chemical structures of the Schiff bases were investigated for their inhibitory activity against BXO.

7.39 (t, 1H, $J = 8.0$ Hz, CH), 7.53 (t, 1H, $J = 8.0$ Hz, arH), 7.72 (d, 1H, $J = 3.6$ Hz, arH), 7.87 (d, 1H, $J = 8.0$ Hz, CH), 7.91 (d, 1H, $J = 8.0$ Hz, arH), 8.02 (d, 1H, $J = 8.0$ Hz, arH), 10.02 (s, 1H, CH), 14.09 (s, 1H, SH). ^{13}C NMR (DMSO-d_6, δppm): 42.51, 111.26, 119.61, 124.61, 128.11, 128.92, 133.60, 133.82, 136.33, 136.64, 145.46, 146.27, 158.44, 162.62. MALDI-TOF-MS: 342.08257 ($[M + 1]^+$). MALDI-TOF-MS: 342.09393 ($[M + 1]^+$), 364.05620 ($[M + Na]^+$).

*3-((1H-Benzo[d][1,2,3]triazol-1-yl)methyl)-4-((4-nitrobenzylidene) amino)-1H-1,2,4-triazole-5(4H)-thione (**8**).*

FT-IR (υ_{max}, cm^{-1}): 3031 (*ar*-CH), 1554, 1587 and 1630 (C = N). ^{1}H NMR (DMSO-d_6, δppm): 6.26 (s, 2H, CH_2), 7.40 (t, 1H, $J = 7.6$ Hz, arH), 7.55 (t, 1H, $J = 8.0$ Hz, arH), 7.88 (d, 1H, $J = 8.0$ Hz, arH), 7.95 (d, 2H, $J = 8.0$ Hz, arH), 8.03 (d, 2H, $J = 8.0$ Hz), 8.27 (d, 2H, $J = 8.0$ Hz, arH), 10.35 (s, 1H, CH), 14.21 (s, 1H, SH). ^{13}C NMR (DMSO-d_6, δppm): 42.57, 111.18, 119.70, 124.47, 124.68, 128.23, 130.05, 133.66, 138.27, 145.45, 146.83, 149.91, 159.48, 162.65. MALDI-TOF-MS: 380.06127 ($[M + 1]^+$). MALDI-TOF-MS: 380.04158 ($[M + 1]^+$).

2.2.2. Computational chemistry (DFT calculations)

Quantum chemistry calculations were performed to gain a better understanding of the molecular geometry and electronic properties of the most active molecules. The density functional theory (DFT) method conjugated to the 6-311G(d,p) basis set was used for all calculations using Gaussian 09 software (Ahmad et al., 2023a,b; Frisch et al., 2009). The absence of imaginary frequencies was checked to confirm the fundamental states.

2.3. Separation of bovine milk

The extraction process was performed according to (Baghiani et al., 2003) with slight modifications, and a total of 1.7 L of milk obtained from a single cow underwent a series of procedures after collection. Initially, it was subjected to centrifugation at 4500 rpm for 35 min. Subsequently, the milk was subjected to multiple separation steps and exposed to varying speeds ranging from 1800 rpm to 4500 rpm at a temperature of + 4 °C (Benarous et al., 2022). The floating cream was collected and resuspended in a solution of K_2HPO_4 (0.2 M) containing 1 mM EDTA, with a volume twice that of the cream (Baghiani et al., 2003). Next, the resulting mixture was stirred for 2 h and then subjected to centrifugation at a speed of 6000 rpm for 20 min (Linani et al., 2021). Finally, the enzyme fraction was successfully acquired, and the resulting float was collected in small aliquots. Furthermore, we lyophilized unprocessed bovine extract that contained xanthine oxidase to prolong the enzyme activity. A volume of 110 ml of enzyme extract was frozen in a deep freezer at a temperature of −50 °C for 1 h. Therefore, the ice water underwent a transition from a solid-state to a gaseous state, which was subsequently eliminated through a process known as “sublimation” at a temperature range of 20–30 °C with P = 0.05 mbar for a total duration of 8 h (Vázquez et al., 2015, Öztürk, 2022).

2.4. Inhibition test

The XO inhibitory assay was carried out by measuring uric acid produced by the oxidation of 0.06 mg/ml xanthine substrate at 505 nm using a Thermo Fisher Scientific microplate reader. In this study, we proposed the use of a double enzyme detection method (DED) to detect uric acid in the form of quinoneimine, which appears as a pink-colored compound. Initially, the samples were dissolved in a small volume of dimethyl sulfoxide (DMSO) (<1%) and subsequently in HEPES buffer (100 mmol/L, pH 8), which was prepared in ultrapure water. A mixture consisting of 20 µL of BXO solution (20 mg/mL) and 20 µL of either a synthetic compound solution or buffer was pre-incubated for 15 min at 37 °C, and the reaction was then initiated by adding 40 µL of xanthine (0.06 mg/ml) to the mixture for 30 min. Finally, the absorbance was read after adding 160 µL of a specific reagent for 20 min. The inhibitory activities of these compounds were compared with allopurinol as a positive control. The XO inhibitory activity was expressed as a percentage of BXO (I%) and calculated using the following formula, in which AC represents the absorbance in the absence of inhibitor and AE represents the absorbance in the presence of the inhibitor (Benarous et al., 2022; Bou-Salah et al., 2020, 2021, Linani et al., 2021, 2022, 2023; Todorov et al., 2021).

$$I\,(\%) = \left(\frac{AC - AE}{AC} \times 100\right)$$

2.5. In silico calculations

2.5.1. Biological activity prediction (PASS)

Numerous research efforts have leveraged the capabilities of PASS software to screen chemical substances for their potential pharmacological effects (Habibyar et al., 2016). In our research, we employed the PASS server to evaluate whether it could accurately identify our leading inhibitors, compounds 4, 7, 9, and 10, as potential xanthine oxidase (XO) inhibitors (Linani et al., 2023). This software was utilized to predict the pharmacological activity of various compounds by employing multilevel neighbors of atoms (MNA) descriptors (Garg and Roy, 2020; Khurana et al., 2011). The predictive analysis was conducted using the structural molecular formulas (SMILES) derived from the ChemOffice v2016 software package. Using this information, the server estimated the potential activity spectrum of the compounds by calculating their probable activity (Pa) and probable inactivity (Pi). This estimation leverages a comprehensive analysis of the structure–activity relationship (SAR) based on a training dataset that includes over 205,000 compounds, each demonstrating a wide range of biological activities encompassing more than 3,750 distinct types (Goel et al., 2011, Jamkhande et al., 2014). Compounds with a Pa value higher than that of Pi are considered potential candidates for specific pharmacological activity (Jamkhande et al., 2014). Additionally, this server has the ability to predict the mechanisms and specific toxicities of molecules, including mutagenicity, carcinogenicity, teratogenicity, and embryotoxicity.

2.5.2. Diagram of absorption, distribution, metabolism, excretion, and toxicity analysis (ADMET)

The assessment of ADMET properties is crucial in the process of drug discovery (Cheng et al., 2012, Idris et al., 2024). Our research concentrated on assessing the ADMET properties of our inhibitors, with the aim of differentiating compounds with drug-like characteristics from those without (Serseg et al., 2022, Ul Islam et al., 2023). To accomplish this goal, we utilized the pre-ADMET v2.0 online server (https://preadmet.qsarhub.com/) and ADMETLab online server (https://admetmesh.scbdd.com/) based on their SMILES extracted from the Chemoffice v2016 package (Linani et al., 2023) (Fig. 2).

2.5.3. Molecular docking

Molecular docking (MD) can help us find the optimal conformation and orientation based on complementarity and pre-organization using a specific algorithm, followed by the application of a scoring function to predict the binding affinity (Fan et al., 2019). Flexible-rigid docking was performed using Autodock Vina software on a DELL sixteen CPU station, allowing full flexibility for the inhibitor and partial flexibility for the receptor (Mari et al., 2018). The receptor (BXO) was acquired from the Protein Data Bank (PDB) with the PDB ID 3nrz (Cao et al., 2010). Bovine xanthine oxidase (BXO), identified by its PDB ID 3nrz, is an enzyme consisting of 1222 amino acids that are further divided into three chains: A (Thr2-Lys165), B (Pro224-Gly528) and C (Asp571-Lys1326). It has a molecular weight of 274 kDa. The active site of 3nrz is a small cavity that is divided into two distinct sections. The first section describes the specificity of the ligand, whether it is a substrate or an inhibitor. The second section is reserved for the binding of cofactors, including flavin adenine dinucleotide (FAD), iron^{2+} sulfide (FES), dioxothiomolybdenum (MOS) and phosphonic acid mono-(2-amino-5,6-dimercapto-4-oxo-

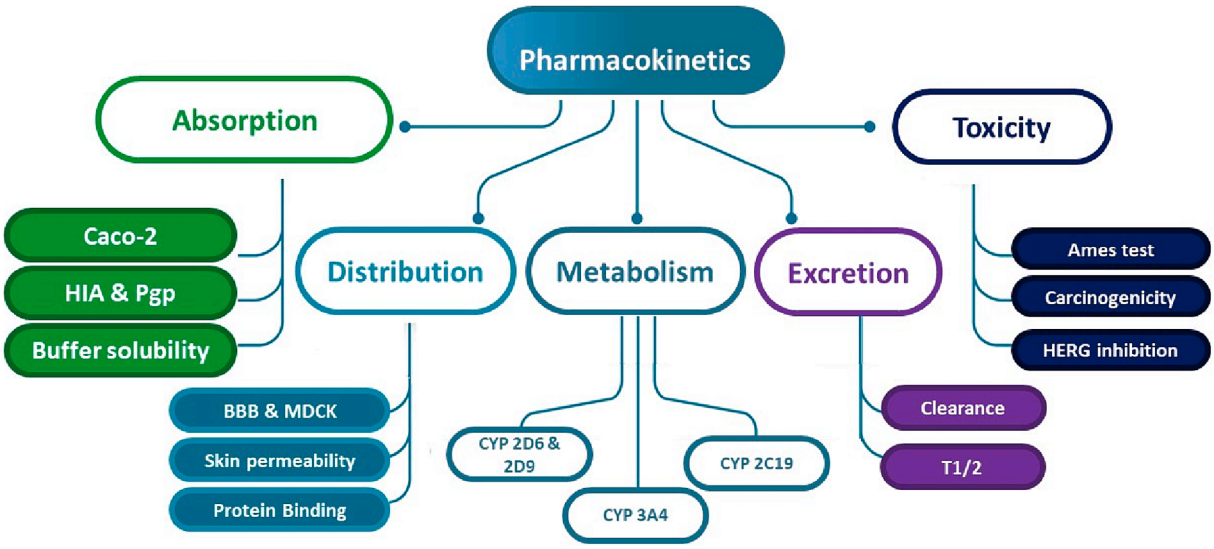

Fig. 2. Workflow of the pharmacokinetic parameters.

3,7,8a,9,10,10a-hexahydro-4 h-8-oxa-1,3,9,10-tetraaza-anthracen-7-yl methyl) ester (MTE) (Bou-Salah et al., 2020). The process of molecular docking involves three primary steps. In the first step, various components, such as ligands, heteroatoms, co-crystallized solvents, and unnecessary water molecules, are removed, excluding those involved in the active site, as defined by Autodock Vina (LINANI et al., 2020). The subsequent step involved adding hydrogens and partial charges using Autodock Tools (ADT) version 1.5.7 (Linani et al., 2022a,b). The final step entails the configuration of the grid box (GB) for the 3nrz center and the size of the binding pocket, which is determined by the grid coordinates x, y, and z. The center of the box is positioned at (x = 37.338, y = 19.791, z = 17.854), with grid points separated by 1 Å located in the middle of the protein (x = 20, y = 22, z = 22). The default settings are generally used, with the exception of the number of conformations, which is set to one. Additionally, the number of docking conformations was set to 10, and the optimal poses were chosen based on their minimal binding energy values in kcal/mol and the ratio of the most frequently repeated poses in percent (%). Finally, Discovery Studio visualizer version 4.0 was utilized to assess the molecular docking outcomes (Serseg et al., 2021; LINANI et al., 2020).

3. Results

3.1. Chemistry

3.1.1. Synthesis

Considering our studies with Schiff bases, these structures, which also contain different heterocyclic rings, have a broad spectrum of activity. Therefore, we evaluated two different groups of Schiff bases that we synthesized previously (Mermer et al., 2019, Mermer and Boulebd, 2023) and 3 new compounds from the first group to study their XO inhibitory activity (Scheme 1). The fact that the first group of compounds had not been studied for any activity before and that the second group of compounds showed promising antioxidant activity led us to this idea. To observe how different structures affect the activity of the newly synthesized compounds (6–8), we tested not only 4-nitrobenzaldehyde, an electron-releasing group but also thiophene and furan rings, which are different heterocyclic structures. The structures of the newly synthesized compounds were characterized by FTIR, NMR and MS spectroscopy methods.

In the FT-IR spectrum of compounds **6–8**, vibration bands in the range of 1630–1638 cm^{-1} attributed to the imine bond formed as a result of the condensation reaction between the amine and the aldehyde were observed. The compounds were found to be in thiol form in the ^{1}H

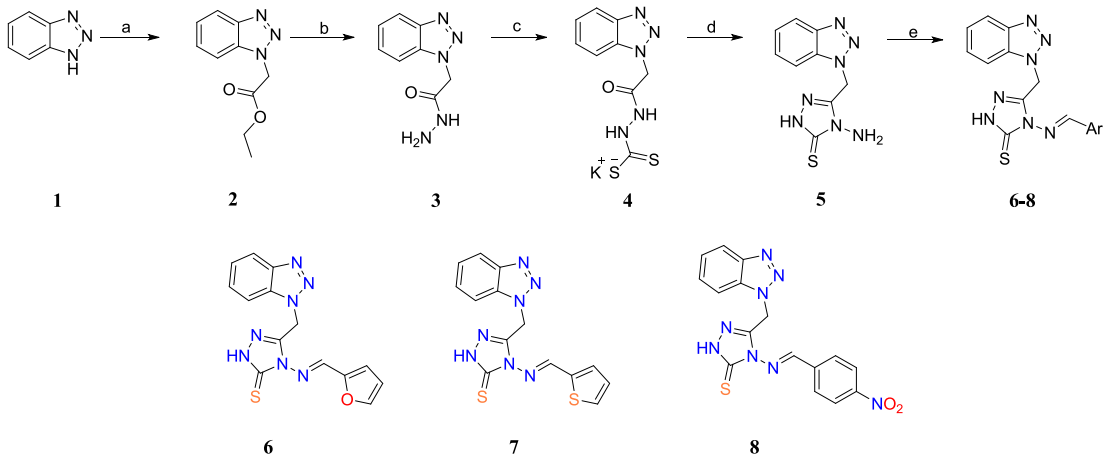

Scheme 1. Synthetic pathway for the target compounds: a) $BrCH_2COOEt$, THF, triethylamine; b) NH_2NH_2, EtOH; c) KOH, CS_2, EtOH; d) NH_2NH_2, H_2O; e) AcOH:H_2O.

NMR spectra, which resonated between 14.06 and 14.21 ppm. The imine (-N = CH) protons also resonated at 9.83, 10.02 and 10.35 ppm. The carbon signals in the compounds were further confirmed by ^{13}C NMR (APT), and it was found that the -N = CH carbons resonated at 151.72, 158.44 and 159.48 ppm. The mass results of the compounds supported the formation of 1,2,4-triazole-Schiff base derivatives with $[M + 1]^+$ ion peaks.

3.1.2. DFT calculations

The molecular geometries of the compounds that yielded the best results (**4, 7, 9** and **10**) were examined through DFT calculations at the B3LYP/6-311G (d,p) level of theory. Initially, a dihedral angle scan was performed along the triazole core bond at 20-degree intervals over 19 steps for both compounds **4** and **7**, as depicted in Fig. 3. The most stable conformation was found with a dihedral angle of 73.28 degrees for compound **4** and 73.27 degrees for compound **7**. Conversely, for molecules **9** and **10**, we studied only the Z configuration, which is known to be more stable than the E configuration. As illustrated in Fig. 3, both compounds exhibit a perfectly planar geometry, which is in line with earlier studies (Amine Khodja and Boulebd, 2021; Djafarou et al., 2023).

Based on these geometries, we calculated the frontier molecular orbitals (FMOs) of the four compounds, and the results are depicted in Fig. 4. FMOs, namely, the highest occupied molecular orbital (HOMO) and lowest unoccupied molecular orbital (LUMO), are crucial orbitals governing the chemical reactivity of molecules. The HOMO identifies the nucleophilic sites of molecules and their ability to donate electrons, while the LUMO, which is a vacant orbital, determines the electrophilic sites and their ability to accept electrons (Boulebd, 2023). The energies of these orbitals serve as valuable indicators of chemical reactivity, particularly the energy difference between the HOMO and LUMO, which governs the overall chemical stability and reactivity of the molecules. As illustrated in Fig. 4, both the HOMO and LUMO of compounds **4** and **7** are localized on the Schiff base and 1,2,4-triazole motifs, signifying that the reactivity of these molecules is influenced by these specific sites. In contrast, the HOMO and LUMO of compounds 9 and **10** are distributed across the entire molecule, indicating that the entire molecule is susceptible to electrophilic and nucleophilic attacks. Additionally, the energy gap (DE) among the compounds decreased in the order of compound **4** > compound **9** > compound **10** > compound **7**, suggesting that compound **4** is the most stable compound, whereas compound **7** is the most reactive.

The electrostatic potential (ESP) is another crucial tool that has been studied, providing valuable insights into the chemical reactivity of a molecule, particularly its interactions with macromolecules. The ESP illustrates the distribution of the electron cloud around a molecule, thereby indicating the electron-richest and electron-poorest regions of molecules. The ESPs of compounds **4**, **7**, **9** and **10** are presented in Fig. 3. Compound **4** contains two electron-poor sites located on the NH and OH groups, along with one electron-rich site around the N of the triazole ring. Similarly, compound **7** displays the same pattern, with the exception of the absence of OH bonds. On the other hand, compounds **9** and **10** feature only one or two significant electron-rich sites situated on the OH and OMe groups and the N atom. However, these molecules lack any prominent electron-poor sites.

3.2. Bovine xanthine oxidase extraction

The yield obtained was 6.43 % of the xanthine oxidase enzyme extract from 1.7 L of bovine milk. The enzyme activity was verified by incubation with xanthine substrate ([xanthine] = 0.06 mg/ml) for 30 min. Then, a specific reagent was added, and the absorbance was read at 505 nm. The appearance of a pink color confirmed the activity of this enzyme.

3.3. Inhibition assay

The synthesized Schiff bases were evaluated for their XO inhibitory effect *in vitro*. The results obtained indicated significant BXO inhibition

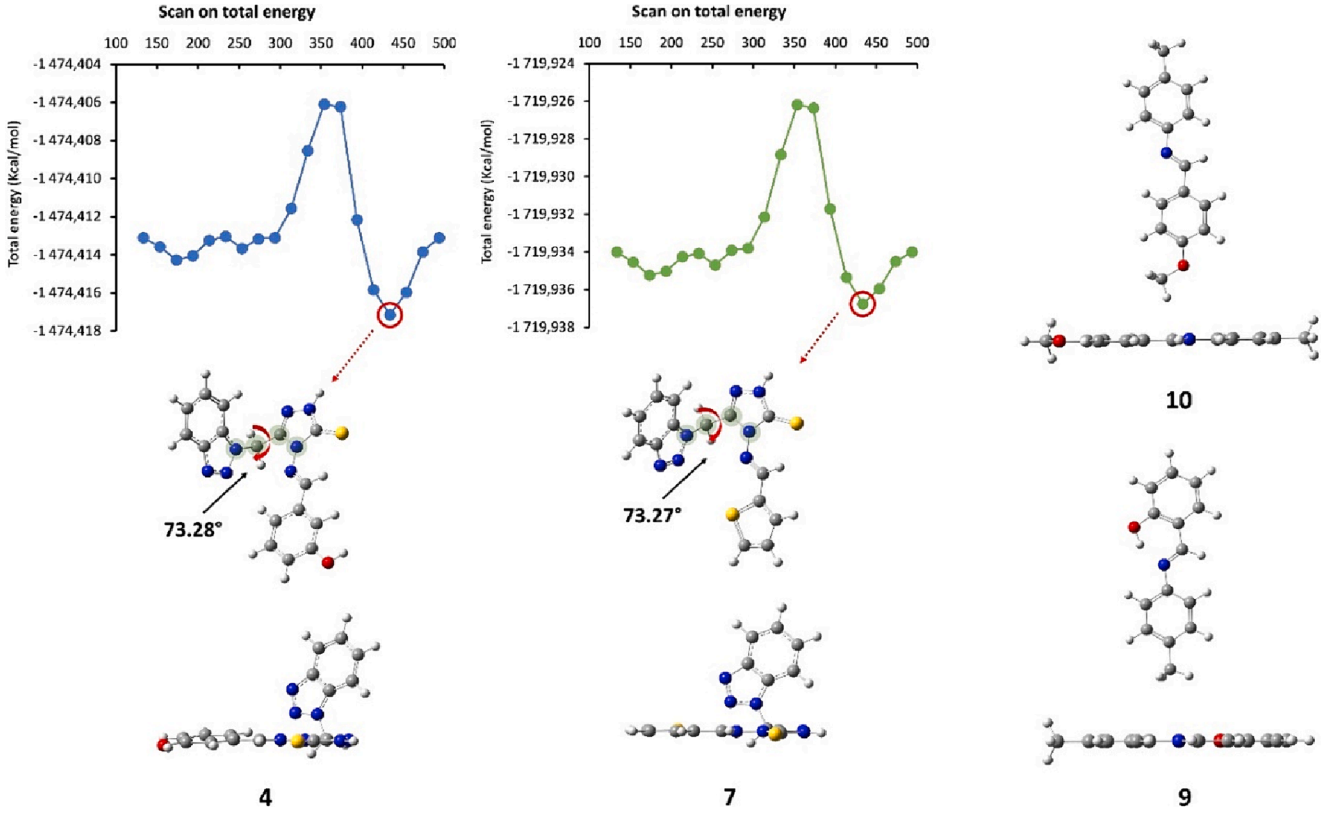

Fig. 3. The total energies of compounds **4** and **7** and the optimized molecular geometries of compounds **9** and **10** were scanned.

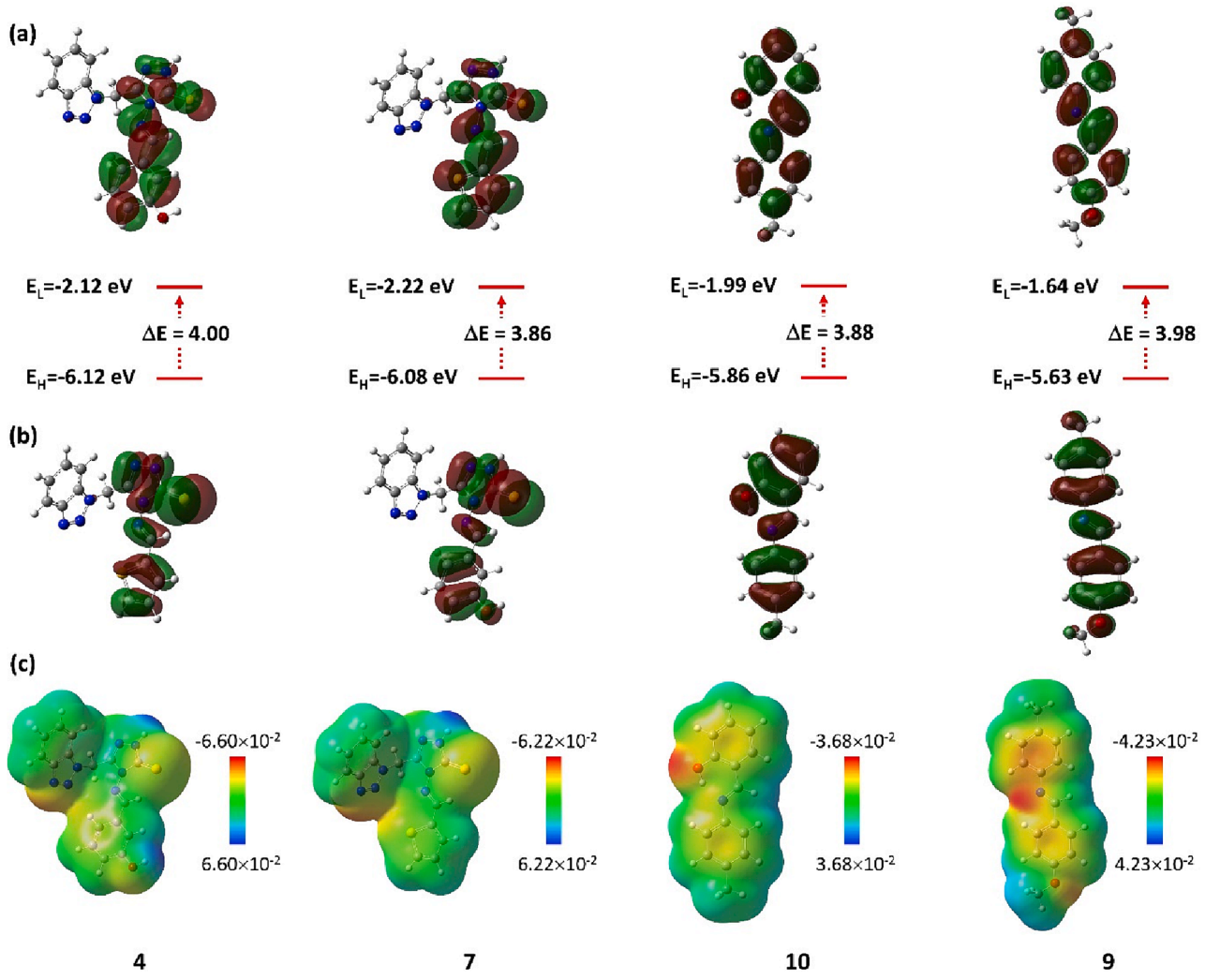

Fig. 4. Energies and distributions of HOMOs (a) and LUMOs (b) as well as ESPs (c) of compounds **4**, **7**, **9** and **10**.

by four synthetic compounds (**4, 7, 9** and **10**) within the IC50 range of 149.56–263.60 μM compared to that of the control Allopurinol (IC50 = 0.84 ± 0.019 μM). The obtained results are summarized in Table 1 and Fig. 5. Moreover, synthetic compounds 1, 2, 3, 5, 6, 8, 11 and 12 exhibited moderate activities, with IC50 values up to 0.1 mg/ml (Fig. 6).

3.4. *In silico calculations*

3.4.1. *Prediction of biological activity*

The biological activity spectra of the best inhibitors were acquired through the use of the online PASS server. The primary objective was to assess the inhibitory effects of these compounds on xanthine oxidase. All the compounds except compound **7** exhibited the predicted xanthine oxidase inhibition activity. All the results are summarized in Table 2.

Table 1
IC50 values of the synthetic compounds and allopurinol.

Compounds	IC50 (μg/ml)	IC50 (μM)
10	31.55 ± 0.91	149.56 ± 4.32
9	41.65 ± 0.46	185.15 ± 2.05
4	89.36 ± 2.96	254.60 ± 8.44
7	89.88 ± 2.39	263.60 ± 7.01
Allopurinol	0.114 ± 0.002	0.84 ± 0.019

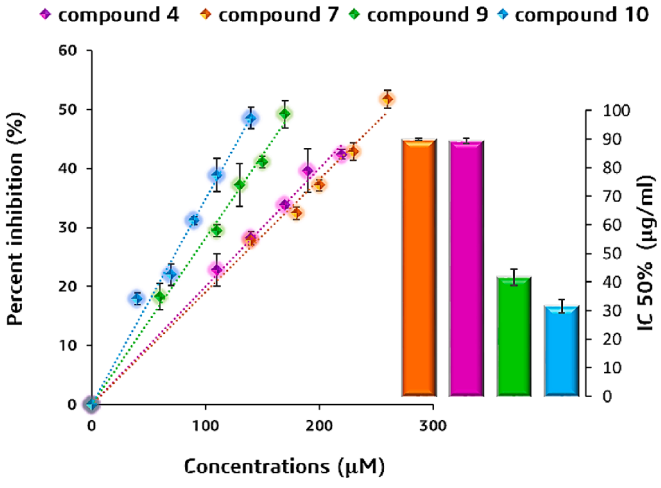

Fig. 5. Curves and IC50 (μg/ml) values of the synthetic compounds against BXO.

3.4.2. *ADMET analysis*

ADMET screening studies have been recognized as fundamental concepts and key tools that were integrated early in the drug discovery phase. These studies served to assist modern project teams in predicting

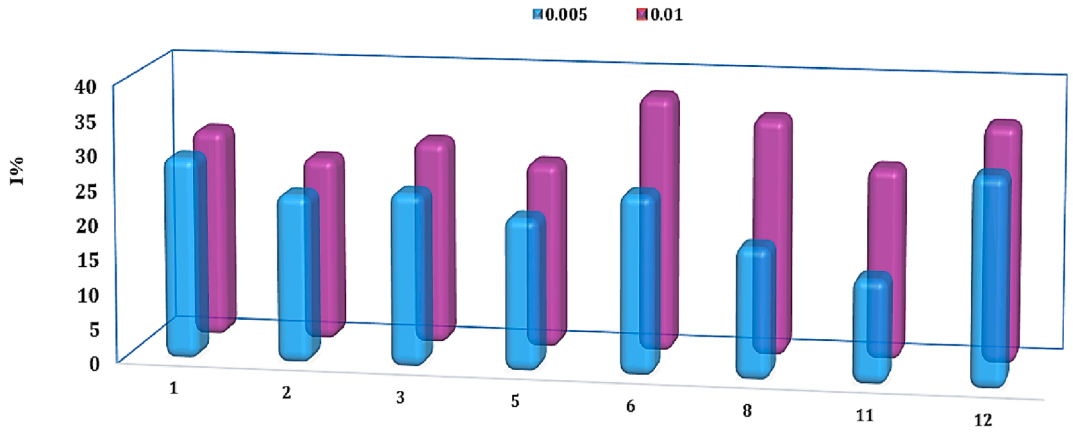

Fig. 6. The percent inhibition of BXO by Schiff base derivatives was moderate.

Table 2
Prediction of the biological activity of the best inhibitors.

Inhibitors	Pa	Pi
10	0.182	0.036
9	0.124	0.068
4	0.127	0.065

human pharmacokinetics and evaluating the potential of drugs (Lin et al., 2003, Ahmad et al., 2023). Different parameters were chosen for ADMET calculations to determine the flux of the best inhibitors within the human body during administration. All the results are depicted in Table 3.

3.4.3. *Molecular docking*

Molecular docking analysis is a computational technique used to predict the binding orientation of a small molecule (ligand) within the binding site of a protein(Abu-Izneid et al., 2024). In this study, the four best inhibitors were docked into bovine xanthine oxidase (PDB ID: 3nrz) to provide a more comprehensive explanation of the inhibitory action of these compounds, and it is necessary to further investigate the mechanism by which they exert their inhibitory effects. The results demonstrated significant interactions between xanthine oxidase and each ligand, indicating a strong binding affinity with the enzyme at a lower energy value than that of the standard compounds. Several hydrophobic interactions were observed, especially amide-π-stacked and π-alkyl interactions, for compounds 10 and 9. Additionally, π-sigma, π-π-stacked, π-π-T-shaped, π-sulfur and π-cation interactions were established for compounds 4 and 7. Most catalytic residues are present, particularly those participating in hydrogen bonds. The detailed molecular docking results are presented in Table 4 and Fig. 7.

4. Discussion

Gout is a disease characterized by acute chronic inflammation caused by the precipitation of monosodium urate crystals in joints, kidneys and subcutaneous sites (Wu et al., 2020). Xanthine oxidase plays a key role in excessive uric acid production (Alghamdi et al., 2021) by the enzymatic conversion of hypoxanthine to xanthine, which is then converted into uric acid (Nguyen et al., 2024). The treatment of gout involves the administration of therapeutic agents such as xanthine oxidase inhibitors (Azmi et al., 2012). Numerous synthetic and natural compounds have been reported as XO inhibitors. (Zafar et al., 2017). In this work, newly synthesized Schiff base derivatives were subjected to a BXO inhibitory activity assay. According to the findings from *in vitro* experiments, compound **10** was the most effective inhibitor, with an IC50 = 149.56 ± 4.32 μM. Compound **9** was the second-best inhibitor, with an IC50 = 185.15 ± 2.05 μM. Both compounds exhibit effective inhibitory activity due to the presence of functional groups such as the imine (-C = N-) group. Additionally, the substitution of methoxy and hydroxyl groups on the phenyl ring plays a crucial role in the inhibitory mechanism. The obtained IC50 values showed that these compounds inhibited BXO better than other synthetic compounds A, B and C, which exhibited IC50 values of 210.7 ± 1.2 μM, 242 ± 6.3 μM and 264.03 ± 4.5 μM, respectively (Zafar et al., 2017). In addition, compounds 4 and **7** showed potent inhibition and ranked third and fourth, with IC50 values of

Table 3
ADMET profiling summarizes the important pharmacokinetic parameters.

Pharmacokinetics	10	9	4	7
Absorption				
Caco-2 cell permeability (nm/sec)	45.11	55.77	20.54	11.99
Human intestinal absorption (HIA %)	96.48	100	96.72	98.71
P-glycoprotein inhibition	Non	Inhibitor	Non	Non
Buffer solubility mg/L	5.70	4.09	70.22	94.99
Distribution				
Blood–brain barrier penetration (C.brain/C. blood)	2.88	0.46	0.42	0.45
MDCK cell permeability (nm/sec)	14.07	1.95	17.35	122.79
Plasma protein binding (%)	100	97.29	89.96	91.77
Skin Permeability	−2.08	−1.98	−3.49	−3.50
Metabolism				
Cytochrome P450 2D6 inhibition	Non	Non	Non	Non
Cytochrome P450 2D6 substrate	Non	Non	Non	Non
Cytochrome P450 3A4 inhibition	Non	Non	Inhibitor	Inhibitor
Cytochrome P450 3A4 substrate	Non	Weakly	Weakly	Substrate
Cytochrome P450 2C19 inhibition	Inhibitor	Inhibitor	Inhibitor	Inhibitor
Cytochrome P450 2C9 inhibition	Inhibitor	Inhibitor	Inhibitor	Inhibitor
Excretion				
Clearance	9.70	6.93	7.27	5.90
$T_{1/2}$	0.46	0.16	0.9	0.8
Toxicity				
Ames test	Mutagen	Mutagen	Mutagen	Mutagen
Carcinogenicity (Mouse)	Positive	Negative	Negative	Negative
Carcinogenicity (Rat)	Positive	Positive	Negative	Negative
HERG-inhibition	Medium-risk	Medium-risk	High-risk	Medium-risk

MDCK: Mandin Darby Canine Kidney; HERG: Human ether-related gene channel.

Table 4
Detailed molecular docking analysis of BXO.

Inhibitors	Energy (Kcal/mol)	Repeating ratio %	Closest residues	Interactions type	Hydrogen bonds	Length (Å)
10	−7.6	100	Arg912, Ala1078, Phe798, Gly799, Gln1040	π-Alkyl π-Sigma Amide-π-Stacked	/	/
9	−7.99	90	Arg912, **Ala910**, Phe798, Gly799, Ala1078, Met1038	π-Alkyl Alkyl π-Sulfur Amide-π-Stacked	/	/
4	−7.7	50	**Glu802**, Lys771, Met770, Pro1076, Leu873, Ala1078, **Leu1014**, **Ala1079**, **Phe914**, Val1011	π-Alkyl π-Sigma π-Sulfur π-Cation π-π-Stacked π-π-T-Shaped	Ser1074 Ser876 **Thr1010** **Phe1009**	3.09 2.61 2.88 3.00
7	−8.37	100	Met770, Lys771, Pro1076, **Glu802**, Leu648, Leu873, **Phe914**, Val1011, **Ala1079**, Ala1078, **Leu1014**, Phe1013	π-Alkyl π-Sulfur π-Cation π-Sigma π-π-Stacked π-π-T-Shaped	Ser876 **Thr1010** **Phe1009**	2.59 2.90 3.14
Allopurinol	−6.15	100	**Phe1009**, Ala1078, **Ala1079**, **Phe914**, **Ala910, Glu802**	π-Alkyl π-Sigma π-π-Stacked π-π-T-Shaped	**Thr1010** **Arg880**	2.81 3.08
Quercetin	−7.5	100	Arg912, Ala1078, Ser1082	π-Alkyl	Thr1083 **Ala1079** Gln1040	> 3.03 3.18 2.57

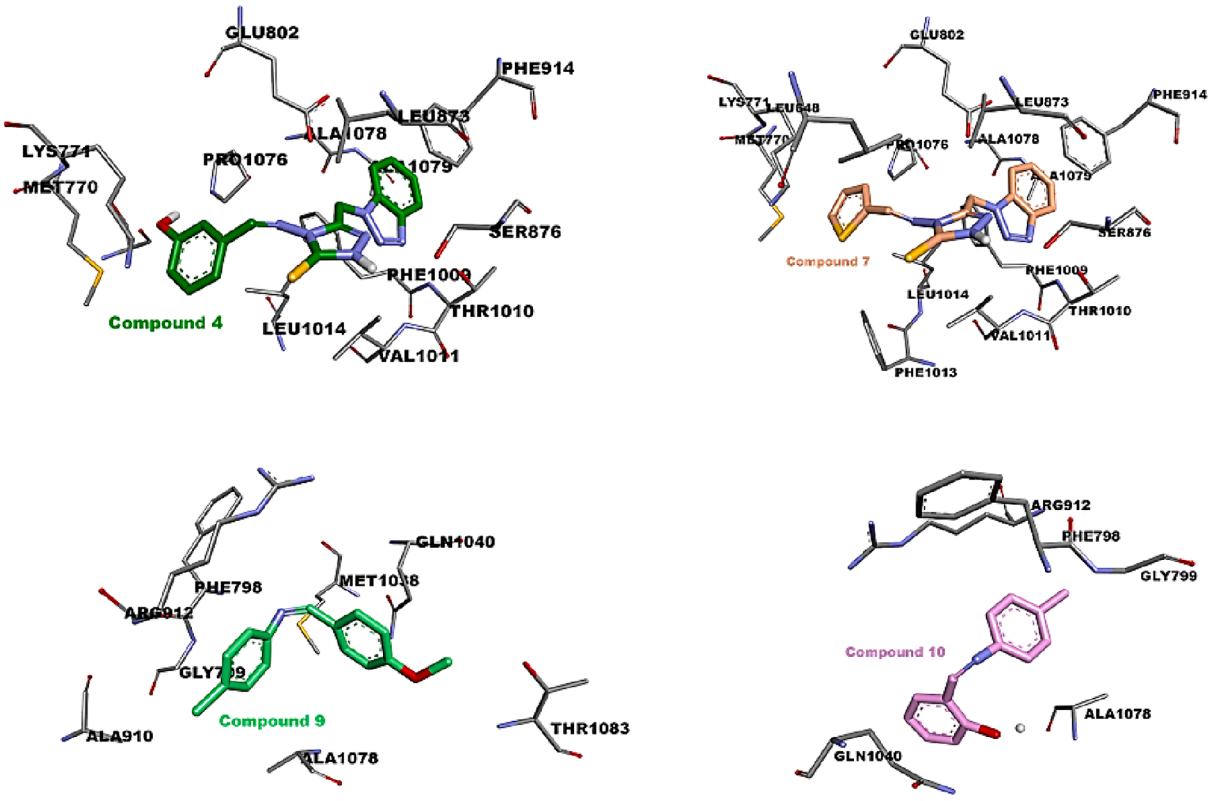

Fig. 7. 3D view of the docked poses of the best inhibitors with different colors indicating interactions with the active site of the BXO residue with the default atom color.

254.60 ± 8.44 μM and 263.60 ± 7.01 μM, respectively. Their activity refers to their specific configuration and incorporation of sulfur and nitrogen heteroatoms in their structure, and their activity was greater than that of compounds D and E, which had IC50 = 330.4 ± 2.1 μM and IC50 = 518.23 ± 2.23 μM, respectively. However, other compounds were investigated for XO inhibition and showed an IC50 of 161 ± 4.5 μM (F) (Zafar et al., 2017) (the structures and names of compounds A, B, C, D, E and F from (Zafar et al., 2017) are found in the supplementary

materials). This study conducted in silico molecular docking analysis to examine the binding interactions between synthetic compounds and xanthine oxidase. For the first inhibitor (Compound **10**), all poses, without exception, are situated within the active site of the enzyme. These poses exhibit identical positioning and interactions with a binding affinity of −7.6 kcal/mol. We observed that 90 % of the interactions were hydrophobic. Thus, no conventional hydrogen bonds were formed**.** The first aromatic ring forms two hydrophobic interactions of π-alkyl type with the amino acids Arg912 and Ala1078. However, the second aromatic ring forms one hydrophobic interaction of the π-sigma type with Gln1040. We also observed that Phe798 and Gly799 participated in the formation of amide-π stacking interactions with this ligand. Concerning the second inhibitor (compound **9**), the presence of two aromatic rings attached to an imine (-C = N-) group is evident in its structure, which is formed through the reaction of an aldehyde or ketone with a primary amine (Mermer et al., 2019). Molecular docking showed that 90 % of the poses were in the active site, exhibiting a strong binding affinity of −7.99 kcal/mol. We observed that the amino acids **Ala910,** Arg912 and Ala1078 play important roles in stabilizing the aromatic ring by forming hydrophobic interactions, especially π-alkyl and alkyl interactions. Furthermore, the sulfur atom of Met 1038 reacts with the aromatic rings to form two π-sulfur interactions with lengths of 5.13 Å and 5.27 Å. Moreover, the presence of the amide group between Phe798 and Gly799 in the active site of the enzyme enables the formation of a significant amide-π stacking interaction. Notably, one catalytic amino acid reacts with this ligand, and no hydrogen interactions have been recorded. Compound **4** is the third best inhibitor. Molecular docking analysis revealed that half of the poses are in the active site and exhibit a tunnel-like structure, which takes the form of a Y-shape with a binding affinity of −7.7 kcal/mol. Four conventional hydrogen bonds were detected, where the hydroxyl group of the phenol ring and the nitrogen atom ported by the 1,2,4-triazole cycle interacted with Ser1074, **Thr1010** and **Phe1009,** resulting in the formation of three hydrogen bonds. Furthermore, the NH group of the 1,2,4-triazole ring forms a conventional hydrogen bond with the hydroxyl group of Ser876 (2.61 Å). The involvement of the phenol ring can also be observed in the formation of two π-sulfur interactions with Met770 and the sulfur atom of the inhibitor. Additionally, a π-cation interaction with Lys771 was formed. The remaining closest residues actively contributed to the formation of eleven hydrophobic π-alkyl, π-sigma, π-π-stacked and π-π-T-shaped interactions. A total of six catalytic amino acids, **Glu802**, **Leu1014**, **Ala1079**, **Phe914**, **Thr1010** and **Phe1009,** were identified to be involved in this inhibitory effect, including those formed through hydrophobic interactions. For the last inhibitor (Compound **7**), the presence of a 1,2,4-triazole ring and an imine (-C = N-) group in its structure, along with specific molecular geometries (Mermer and Boulebd, 2023), leads to the establishment of a considerable number of interactions. Thus, the incorporation of nitrogen and sulfur heteroatoms within its structure plays a crucial role in the inhibitory action of six catalytic amino acids (**Glu802, Phe914, Ala1079, Thr1010, Phe1009** and **Leu1014**) reacting with this ligand. Molecular docking analysis indicated that all the poses were successfully docked within the active site, with each pose exhibiting a similar position and interaction with the BXO residue. Therefore, the best binding affinity was −8.37 kcal/mol. The nitrogen atom carried by the 1,2,4-triazole cycle interacted with **Thr1010** and **Phe1009,** forming two conventional hydrogen bonds with lengths of 2.90 Å and 3.14 Å, respectively. Furthermore, a very strong hydrogen bond was observed between the NH of the 1,2,4-triazole cycle and the hydroxyl group of Ser876, with a length of 2.59 Å. As a result, three hydrogen bonds were formed with this inhibitor. On the other hand, the thiophene cycle participates in the formation of two π-sulfur interactions with the benzene ring of Phe1013 and the sulfur group of Met770, as well as one π-cation interaction with Lys771. Therefore, Pro1076, Leu648, Leu873, **Phe914**, Val1011, **Ala1079**, Ala1078, **Leu1014**, Lys771 and **Phe1009** were the amino acids with the most interactions, with thirteen hydrophobic interaction types of π-alkyl, π-sigma, π-π-stacked and π-π-T-shaped interactions and various interatomic distances. We observed that **Glu802** participated in carbon–hydrogen interactions. The strong binding of the inhibitor to the enzyme can be attributed to the numerous interactions formed with the catalytic amino acids; these interactions elucidate the high affinity of the inhibitor. In comparison to the docking results of allopurinol complexed with BXO (PDB ID: 3bdj), we observed that allopurinol exhibited a limited number of interactions. It only forms two hydrogen bonds with a greater length (greater than 2.81 Å). No evidence of π-cation or π-sulfur intermolecular interactions was found, indicating that the remaining interactions were hydrophobic. On the other hand, our inhibitors react with most catalytic amino acids. Additionally, they exhibit a diverse and stronger range of interactions due to the presence of functional groups such as imine (-C = N-) groups, NH, OH, and SH groups and the presence of heterocycles such as 1,2,4-triazole.

The *in vitro* results were also supported by the predictions of many other measurements. ADMET prediction revealed that compound **10** has a beneficial absorption profile. The blood–brain barrier penetration was acceptable. However, it has the ability to strongly bind to plasma proteins with high passive permeability to MDCK cells. The toxicity profile shows mutagenicity to the Ames test and carcinogenicity to both mice and rats. It poses a moderate risk for human ether-related gene channel inhibition. Compound **9** has an optimal Caco-2 cell permeability and human intestinal level, indicating a strong tendency to penetrate these cells. However, it cannot easily pass through the blood–brain barrier or through MDCK cells. The toxicity profile shows mutagenicity in the AMES test and observed carcinogenicity in rats, with a medium risk for HERG. The third compound (Compound **4**) achieved acceptable Caco-2 cell permeability and intestinal absorption. Nevertheless, it penetrates the blood–brain barrier slowly. In terms of toxicity, it can inhibit the human ether-related gene channel (HERG). Therefore, it can be dangerous for cardiovascular patients. No indication of carcinogenicity risk was detected. Compared with the other inhibitors, compound **7** has the lowest caco-2 cell permeability and blood–brain barrier penetration, and its human intestinal absorption is considered suitable. Additionally, compound **7** exhibits a toxicity profile similar to that of compound **4**, with a medium risk for HERG. Notably, none of these synthetic compounds exhibited inhibitory activity against Cytochrome P450 2D6 or 3A4. However, they do display inhibitory activity toward Cytochrome P450 2C9 and 2C19. In terms of excretion, all the compounds displayed moderate clearance with a long half-life.

PASS analyses based on molecular smiles confirmed the efficacy of these compounds as xanthine oxidase inhibitors. The first best inhibitor (compound **10)** had a greater number of predicted biological activities (1745) than the other compounds, with xanthine oxidase inhibition values of Pa = 0.182 and Pi = 0.036. For compound **9**, we registered a number of predicted biological activities of 1250. The Pa and Pi values for XO inhibition were 0.124 and 0.068, respectively. Concerning the third best inhibitor (compound **4),** we observed 61 biological activities with XO inhibition values of Pa = 0.127 and Pi = 0.065.

5. Conclusion

This research has successfully identified a novel class of Schiff base derivatives as potent inhibitors of bovine xanthine oxidase (XO), employing both *in vitro* and in silico screening methods. Among the tested compounds, compounds 10, 9, 4, and 7 were the most effective, demonstrating IC50 values ranging from 149.56 μM to 263.60 μM. These findings were further validated through in silico studies, which revealed a consistent pattern of interactions between these inhibitors and the critical residues of the enzyme. Additionally, these synthetic compounds have shown promising ADMET profiles, underscoring their potential for in vivo applications. Consequently, it is crucial to consider various factors for their effective translation into therapeutic agents.

CRediT authorship contribution statement

Fatna Bellahcene: Data curation, Formal analysis, Methodology, Writing – original draft. **Khedidja Benarous:** Conceptualization, Data curation, Formal analysis, Investigation, Methodology, Project administration, Resources, Software, Supervision, Validation, Visualization, Writing – original draft, Writing – review & editing. **Arif Mermer:** Conceptualization, Data curation, Formal analysis, Investigation, Methodology, Resources, Supervision, Validation, Visualization, Writing – original draft, Writing – review & editing. **Houssem Boulebd:** Software, Visualization, Writing – original draft, Conceptualization, Data curation, Investigation, Methodology. **Talia Serseg:** Data curation, Resources. **Abderahmane Linani:** Formal analysis, Resources, Validation. **Alaeddine Kaouka:** Project administration, Resources, Software. **Mohamed Yousfi:** Investigation, Project administration, Resources. **Asad Syed:** Formal analysis, Funding acquisition. **Abdallah M. Elgorban:** Formal analysis, Funding acquisition. **Yasuhiro Ozeki:** Funding acquisition, Validation. **Sarkar M.A. Kawsar:** Funding acquisition, Writing – review & editing.

Declaration of competing interest

The authors declare that they have no known competing financial interests or personal relationships that could have appeared to influence the work reported in this paper.

Acknowledgment

The authors extend their appreciation to the Researchers Supporting Project number (RSP2024R56), King Saud University, Riyadh, Saudi Arabia.

Appendix A. Supplementary material

Supplementary data to this article can be found online at https://doi.org/10.1016/j.jsps.2024.102062.

References

Abu-Izneid, T., Rauf, A., Ahmad, Z., et al., 2024. Density functional theory (DFT), molecular docking, and xanthine oxidase inhibitory studies of dinaphthodiospyrol S from Diospyros kaki L. Saudi Pharma. J. 32, 101936.

Ahmad, S., Khan, M., Rehman, N.U., et al., 2022a. Design, synthesis, crystal structure, in vitro and in silico evaluation of new N'-benzylidene-4-tert-butylbenzohydrazide derivatives as potent urease inhibitors. Molecules (Basel, Switzerland) 27. https://doi.org/10.3390/molecules27206906.

Ahmad, S., Khan, M., Shah, M.I.A., et al., 2022b. Synthetic transformation of 2-{2-fluoro [1,1'-biphenyl]-4-yl} propanoic acid into hydrazide-hydrazone derivatives. In vitro urease inhibition and in silico study. ACS Omega 7, 45077–45087. https://doi.org/10.1021/acsomega.2c05498.

Ahmad, R., Khan, M., Alam, A., et al., 2023a. Synthesis, molecular structure and urease inhibitory activity of novel bis-Schiff bases of benzyl phenyl ketone: A combined theoretical and experimental approach. Saudi Pharma. J. : SPJ : Off. Publ. Saudi Pharma. Soc. 31, 101688 https://doi.org/10.1016/j.jsps.2023.06.021.

Ahmad, S., Khan, M., Alam, A., et al., 2023b. Novel flurbiprofen clubbed oxadiazole derivatives as potential urease inhibitors and their molecular docking study. RSC Adv. 13, 25717–25728.

Alghamdi, A. A., Althumali, J. S., Almalki, M. M. M., et al., 2021. An Overview on the Role of Xanthine Oxidase Inhibitors in Gout Management. 12, 94-99.

Amine Khodja, I., Boulebd, H., 2021. Synthesis, biological evaluation, theoretical investigations, docking study and ADME parameters of some 1,4-bisphenylhydrazone derivatives as potent antioxidant agents and acetylcholinesterase inhibitors. Mol. Divers. 25, 279–290. https://doi.org/10.1007/s11030-020-10064-8.

Azim, T., Wasim, M., Akhtar, M.S., et al., 2021. An in vivo evaluation of anti-inflammatory, analgesic and anti-pyretic activities of newly synthesized 1, 2, 4 Triazole derivatives. BMC Complement. Med. Ther. 21, 1–15.

Azmi, S. M. N., Jamal, P. and Amid, A. J. i. f. r. j., 2012. Xanthine oxidase inhibitory activity from potential Malaysian medicinal plant as remedies for gout. 19, 159-165.

Baghiani, A., Harrison, R., Benboubetra, M. J. A. o. P., et al., 2003. Purification and partial characterisation of camel milk xanthine oxidoreductase. 111, 407-414.

Benarous, K., Bou-Salah, L., Linani, A., et al., 2022. Lanthanide (III) complexes of bis-coumarins as strong inhibitors of bovine xanthine oxidase-molecular docking and SAR studies. J. Biomol. Struct. Dyn. 40, 2733–2739.

Boulebd, H.J.P., 2023. Insights on the antiradical capacity and mechanism of phytocannabinoids: H-abstraction and electron transfer processes in physiological media and the influence of the acid-base equilibrium. Phytochemistry 208, 113608.

Boulechfar, C., Ferkous, H., Delimi, A., et al., 2023. Schiff bases and their metal Complexes: A review on the history, synthesis, and applications. Inorg. Chem. Commun. 150, 110451 https://doi.org/10.1016/j.inoche.2023.110451.

Bou-Salah, L., Benarous, K., Linani, A., et al., 2020. In vitro and in silico inhibition studies of five essential oils on both enzymes human and bovine xanthine oxidase. Indus. Crops Prod. 143, 111949.

Bou-Salah, L., Benarous, K., Linani, A., et al., 2021. Anti-inflammatory drugs as new inhibitors to xanthine oxidase: in vitro and in silico approach. Mol. Cell. Probes 58, 101733.

Cao, H., Pauff, J. M. and Hille, R. J. J. o. B. C., 2010. Substrate orientation and catalytic specificity in the action of xanthine oxidase: the sequential hydroxylation of hypoxanthine to uric acid. 285, 28044-28053.

Cheng, F., Li, W., Zhou, Y., et al., 2012. admetSAR: a comprehensive source and free tool for assessment of chemical ADMET properties. ACS Publications.

Dalbeth, N., Gosling, A. L., Gaffo, A., et al., 2021. Gout. Lancet (London, England). 397, 1843-1855. https://doi.org/10.1016/s0140-6736(21)00569-9.

Djafarou, S., Mermer, A., Barut, B., et al., 2023. Synthesis and evaluation of the antioxidant and anti-tyrosinase activities of thiazolyl hydrazone derivatives and their application in the anti-browning of fresh-cut potato. Food Chem. 414, 135745.

Dong, Y., Li, M., Hao, Y., et al., 2023. Antifungal Activity, Structure-Activity Relationship and Molecular Docking Studies of 1, 2, 4-Triazole Schiff Base Derivatives. 20, e202201107.

Fan, J., Fu, A., Zhang, L., 2019. Progress in molecular docking. Quantitative Biol. 7 https://doi.org/10.1007/s40484-019-0172-y.

M. J. Frisch, G. W. T., H. B. Schlegel, G. E. Scuseria, M. A. Robb, J. R. Cheeseman, G. Scalmani, V. Barone, B. Mennucci, G. A. Petersson, H. Nakatsuji, M. Caricato, X. Li, A.F.I. H. P. Hratchian, J. Bloino, G. Zheng,, M.H. J. L. Sonnenberg, M. Ehara, K. Toyota,, J.H. R. Fukuda, M. Ishida, T. Nakajima, Y. Honda,, H.N. O. Kitao, T. Vreven, J. A. Montgomery Jr,, F.O. J. E. Peralta, M. J. Bearpark, J. Heyd,, K.N.K. E. N. Brothers, V. N. Staroverov, R. Kobayashi,, K.R. J. Normand, A. P. Rendell, J. C. Burant,, J.T. S. S. Iyengar, M. Cossi, N. Rega, N. J. Millam,, J.E.K. M. Klene, J. B. Cross, V. Bakken, C. Adamo,, R.G. J. Jaramillo, R. E. Stratmann, O. Yazyev,, R.C. A. J. Austin, C. Pomelli, J. W. Ochterski,, K.M. R. L. Martin, V. G. Zakrzewski, G. A. Voth,, J.J.D. P. Salvador, S. Dapprich, A. D. Daniels,, J.B.F.¨O. Farkas, J. V. Ortiz, J. Cioslowski,, D. J. , 2009. Fox, Gaussian 09, . Gaussian Inc., Wallingford CT.

Garg, S., Roy, A., 2020. In silico analysis of selected alkaloids against main protease (M (pro)) of SARS-CoV-2. Chem. Biol. Interact. 332, 109309 https://doi.org/10.1016/j.cbi.2020.109309.

Goel, R.K., Singh, D., Lagunin, A., et al., 2011. PASS-assisted exploration of new therapeutic potential of natural products. Med. Chem. Res. 20, 1509–1514.

Habibyar, A. F., Sharma, N. and Khurana, N. J. E. J. o. P., 2016. PASS assisted prediction and pharmacological evaluation of hesperidin against scopolamine induced amnesia in mice. 789, 385-394.

Idris, S., Jan, F., Waheed, M., et al., 2024. Multifaceted bioactivity of thiosemicarbazide derivatives: Synthesis, characterization, and DFT investigations on inhibition of α-amylase, hydroxyl radical scavenging, and iron chelating activities with molecular docking insights. J. Mol. Struct. 1304, 137669 https://doi.org/10.1016/j.molstruc.2024.137669.

Jamkhande, P.G., Wattamwar, A.S., Pekamwar, S.S., et al., 2014. Antioxidant, antimicrobial activity and in silico PASS prediction of Annona reticulata Linn. root extract. Beni-Suef Univ. J. Basic Appl. Sci. 3, 140–148.

Jumaa, F., Tapabashi, N. and Abd, O., 2017. Synthesis and Characterization of some 5, 5-Ethyl Bis-(4-Amino-4H-1, 2, 4-Triazole-3-Thiol) Derivatives.

Khan, M., Fazal, Z., Alam, A., et al., 2023. Synthetic transformation of 4-fluorobenzoic acid to 4-fluorobenzohydrazide Schiff bases and 1, 3, 4-oxadiazole analogs having DPPH radical scavenging potential. Lett. Drug Des. Discov. 20, 2018–2024.

Khurana, N., Ishar, M.P.S., Gajbhiye, A., et al., 2011. PASS assisted prediction and pharmacological evaluation of novel nicotinic analogs for nootropic activity in mice. Eur. J. Pharmacol. 662, 22–30.

Kim, S.J., Kim, M.G., Kim, J., et al., 2023. Bioprinting methods for fabricating in vitro tubular blood vessel models. Cyborg Bionic Syst. (Washington D.C.) 4, 0043. https://doi.org/10.34133/cbsystems.0043.

Li, X., Li, X.-Q., Liu, H.-M., et al., 2012. Synthesis and evaluation of antitumor activities of novel chiral 1, 2, 4-triazole Schiff bases bearing γ-butenolide moiety. Org. Med. Chem. Lett. 2, 1–5.

Lin, J., Sahakian, D.C., de Morais, S.M., et al., 2003. The role of absorption, distribution, metabolism, excretion and toxicity in drug discovery. Curr. Top. Med. Chem. 3, 1125–1154. https://doi.org/10.2174/1568026033452096.

Linani, A., Benarous, K., Bou-Salah, L., et al., 2021. Hispidin, Harmaline, and Harmine as potent inhibitors of bovine xanthine oxidase: Gout treatment, in vitro, ADMET prediction, and SAR studies. Bioorg. Chem. 112, 104937.

Linani, A., Benarous, K., Bou-Salah, L., et al., 2022a. Exploring structural mechanism of COVID-19 treatment with glutathione as a potential peptide inhibitor to the main protease: Molecular dynamics simulation and MM/PBSA free energy calculations study. Int. J. Peptide Res. Ther. 28, 55.

LINANI, A., BENAROUS, K. and Yousfi, M., 2020. Novel Structural Mechanism of Glutathione as a potential peptide inhibitor to the main protease (Mpro): CoviD-19 treatment, Molecular docking and SAR study.

Linani, A., Benarous, K., Bou-Salah, L., et al., 2022. The inhibitory kinetics of vitamins B9, C, E, and D3 on bovine xanthine oxidase: Gout treatment. 359, 109922.

Linani, A., Serseg, T., Benarous, K., et al., 2023. Cupressus sempervirens L. flavonoids as potent inhibitors to xanthine oxidase: in vitro, molecular docking, ADMET and PASS

studies. J. Biomol. Struct. Dyn. 41, 7055–7068. https://doi.org/10.1080/07391102.2022.2114943.
Luo, G., Zhou, Z., Huang, C., et al., 2023. Itaconic acid induces angiogenesis and suppresses apoptosis via Nrf2/autophagy to prolong the survival of multi-territory perforator flaps. Heliyon 9, e17909. https://doi.org/10.1016/j.heliyon.2023.e17909.
Mari, K. R., Muthukrishnan, S. J. J. o. P. and Phytochemistry, 2018. Structural characterization and insilico study on Pisonia alba Leaves extract. 7, 681-693.
Matela, G. J. A.-C. A. i. M. C., 2020. Schiff bases and complexes: a review on anti-cancer activity. 20, 1908-1917.
Mermer, A., Boulebd, H., 2023. An eco-friendly method for the synthesis of 1,2,4-triazole-Schiff base derivatives in aqueous medium and DFT calculations. J. Mol. Struct. 1271, 134102 https://doi.org/10.1016/j.molstruc.2022.134102.
Mermer, A., Demirbas, N., Uslu, H., et al., 2019. Synthesis of novel Schiff bases using green chemistry techniques; antimicrobial, antioxidant, antiurease activity screening and molecular docking studies. J. Mol. Struct. 1181, 412–422. https://doi.org/10.1016/j.molstruc.2018.12.114.
Newberry, S.J., FitzGerald, J.D., Motala, A., et al., 2017. Diagnosis of gout: a systematic review in support of an American College of Physicians Clinical Practice Guideline. Ann. Internal Med. 166, 27–36.
Nguyen, D.-K., Liu, T.-W., Hsu, S.-J., et al., 2024. Xanthine oxidase inhibition study of isolated secondary metabolites from Dolichandrone spathacea (Bignoniaceae): In vitro and in silico approach. 101980.
Nuriye Tuna, S., 2022. Overview of Schiff Bases. Schiff Base in Organic, Inorganic and Physical Chemistry. Takashiro, A. Rijeka, IntechOpen: Ch. 2.
Öztürk, H.İ., 2022. The effect of different lyophilisation pressures on the microbiological stability, physicochemical, microstructural, and sensorial properties of yoghurt powders. Int. Dairy J. 129, 105347 https://doi.org/10.1016/j.idairyj.2022.105347.
Raczuk, E., Dmochowska, B., Samaszko-Fiertek, J., et al., 2022. Different Schiff bases-structure, importance and classification. Molecules (Basel, Switzerland) 27. https://doi.org/10.3390/molecules27030787.
Saadaoui, I., Krichen, F., Salah, B. B., et al., 2019. Design, synthesis and biological evaluation of Schiff bases of 4-amino-1, 2, 4-triazole derivatives as potent angiotensin converting enzyme inhibitors and antioxidant activities. 1180, 344-354.
Serseg, T., Benarous, K., Serseg, M., et al., 2022. Discovery of inhibitors against SARS-CoV-2 associated fungal coinfections via virtual screening, ADMET evaluation, PASS, molecular docking, dynamics and pharmacophore studies. Arab. J. Basic Appl. Sci. 29, 337–350.
Serseg, T., Benarous, K. and Yousfi, M. J. C. c.-a. d. d., 2021. Hispidin and Lepidine E: two Natural Compounds and Folic acid as Potential Inhibitors of 2019-novel coronavirus Main Protease (2019-nCoVMpro), molecular docking and SAR study. 17, 469-479.
Shilpa Laxman, S., 2022. Introduction to Schiff Base. Schiff Base in Organic, Inorganic and Physical Chemistry. Takashiro, A. Rijeka, IntechOpen: Ch. 1.
Todorov, L., Saso, L., Benarous, K., et al., 2021. Synthesis, structure and impact of 5-aminoorotic acid and its complexes with lanthanum (III) and gallium (III) on the activity of xanthine oxidase. 26, 4503.
Ul Islam, A., Serseg, T., Benarous, K., et al., 2023. Synthesis, antimicrobial activity, molecular docking and pharmacophore analysis of new propionyl mannopyranosides. J. Mol. Struct. 1292, 135999 https://doi.org/10.1016/j.molstruc.2023.135999.
Vázquez, C.V., Rojas, M.G., Ramírez, C.A., et al., 2015. Total phenolic compounds in milk from different species. Design of an extraction technique for quantification using the Folin-Ciocalteu method. Food Chem. 176, 480–486. https://doi.org/10.1016/j.foodchem.2014.12.050.
Wu, M., Tian, Y., Wang, Q., et al., 2020. Gout: A disease involved with complicated immunoinflammatory responses: A narrative review. Clin. Rheumatol. 39, 2849–2859.
Yu, Z., Cao, Y., Kan, R., et al., 2022. Identification of egg protein-derived peptides as xanthine oxidase inhibitors: Virtual hydrolysis, molecular docking and in vitro activity evaluation. Food Sci. Hum. Wellness 11, 1591–1597.
Zafar, H., Hayat, M., Saied, S., et al., 2017. Xanthine oxidase inhibitory activity of nicotino/isonicotinohydrazides: a systematic approach from in vitro, in silico to in vivo studies. 25, 2351-2371.
Zhao, Y., Chen, S., Shen, F., et al., 2019. In vitro neutralization of autocrine IL-10 affects Op18/stathmin signaling in non-small cell lung cancer cells. Oncol. Rep. 41, 501–511. https://doi.org/10.3892/or.2018.6795.
Zhao, Q., Meng, Y., Liu, J., et al., 2022. Separation, identification and docking analysis of xanthine oxidase inhibitory peptides from pacific cod bone-flesh mixture. LWT 167, 113862.
Zhou, L., Liu, Y., Sun, H., et al., 2022. Usefulness of enzyme-free and enzyme-resistant detection of complement component 5 to evaluate acute myocardial infarction. Sens. Actuators B: Chem. 369, 132315 https://doi.org/10.1016/j.snb.2022.132315.